PHYSICAL REVIEW B **82**, 104206 (2010)

# Local atomic structure of Ca-Mg-Zn metallic glasses

O. N. Senkov,[1,*] D. B. Miracle,[1] E. R. Barney,[2] A. C. Hannon,[2] Y. Q. Cheng,[3] and E. Ma[3]
[1]*Air Force Research Laboratory, Materials and Manufacturing Directorate, Wright-Patterson Air Force Base, Ohio 45433, USA*
[2]*ISIS Facility, Rutherford Appleton Laboratory, Chilton, Didcot, Oxon OX11 0QX, United Kingdom*
[3]*Department of Materials Science and Engineering, John Hopkins University, Baltimore, Maryland 21218, USA*
(Received 20 May 2010; revised manuscript received 16 July 2010; published 16 September 2010)

The amorphous structure of four $\mathrm{Ca}_{60}\mathrm{Mg}_X\mathrm{Zn}_{40-X}$ ($X=10$, 15, 20, and 25 at. %) ternary metallic glasses (MGs) has been investigated by neutron and x-ray diffraction, using Reverse Monte Carlo modeling to simulate the results. A critical analysis of the resultant models, corroborated by *ab initio* molecular-dynamics simulations, indicate that the glass structure for this system can be described as a mixture of Mg- and Zn-centered clusters, with Ca dominating in the first coordination shell of these clusters. A coordination number (CN) of 10 [with about 7 Ca and 3 (Mg+Zn) atoms] is most common for the Zn-centered clusters. CN=11 and 12 [with about 7–8 Ca and 4 (Mg+Zn) atoms] are most common for Mg-centered clusters. Fivefold bond configurations (pentagonal pyramids) dominate (~60%) in the first coordination shell of the clusters, suggesting dense atomic packing. Bond-angle distributions suggest near-equilateral triangles and pentagonal bipyramids to be the most common nearest atom configurations. This is the systematic characterization of the structure of Ca-Mg-Zn MGs, a category of bulk MGs with interesting properties and intriguing applications. It is also the experimental verification of the principle of efficient packing of solute-centered clusters in ternary MGs.

DOI: 10.1103/PhysRevB.82.104206 PACS number(s): 61.43.Dq, 61.05.fm, 61.43.Bn, 83.10.Rs

## I. INTRODUCTION

The recently discovered ternary Ca-Mg-Zn, Ca-Mg-Cu, and Ca-Mg-Al bulk metallic glasses (BMGs) have unique properties that distinguish them from other BMGs.[1–5] They are based on two simple metal elements, Ca and Mg, and have the lowest density (in the range of 1.6–2.4 g/cm$^3$) among all currently known BMGs.[6] These metallic glasses also have extremely low Young's (~20–30 GPa) and shear (~9–14 GPa) moduli, comparable with the moduli of human bones.[7] Some of these ternary alloys have extremely good glass-forming ability (GFA), similar to the GFA of the best Zr-based BMGs.[4,6,8]

Figure 1 shows the liquidus projection in the Ca-rich corner of the Ca-Mg-Zn system.[9] The compositions of the ternary Ca-Mg-Zn amorphous alloys reported in Refs. 2 and 4 are marked as solid circles and their critical plate thicknesses are shown by corresponding numbers (in mm). The presence of a ternary eutectic reaction provides a strong liquidus temperature gradient in the selected composition area, which leads to high sensitivity of GFA on alloy composition. For example, the maximum plate thickness at which an alloy is fully amorphous after casting in a water-cooled copper mold, can be increased from 0.5 mm to 6–10 mm within a composition range of only 5%.[4] Thermodynamic analysis of the onset driving force (ODF) for crystallization of different phases in the Ca-Mg-Zn system has shown[10] that the GFA of the ternary alloys improves with a decrease in the ODF of competing intermetallic phases [for example, CaZn (at $X \leq 17.5$ at. %) and $\mathrm{CaMg}_2$ (at $X > 17.5$ at. %) for $\mathrm{Ca}_{60}\mathrm{Mg}_X\mathrm{Zn}_{40-X}$ alloys, see Fig. 2].

Recent structural analysis of metal-metal-type BMGs has focused on those based on transition metals such as Zr-Cu (Refs. 11 and 12) and Zr-Cu-Al.[13] Many papers discuss the icosahedral local structures in these BMGs and the importance of these motifs on relaxation dynamics, GFA and deformation properties. However, icosahedral order is not universally the dominant short-range order (SRO) in metallic glasses. For example, transition-metal-metalloid metallic glasses [such as those based on Fe-C or Ni-B (Refs. 14 and 15)], and many Al-transition-metal glasses (with high Al content[16]), are not characterized by icosahedral SRO.

Ca-Mg-Zn represents a different group of metal-metal-type BMGs based on alkaline-earth metals, for which the glass structure has not been systematically studied so far, although a few examples for Mg-Cu-based MGs have been reported.[17,18] Based on relative atomic sizes[19] and the effi-

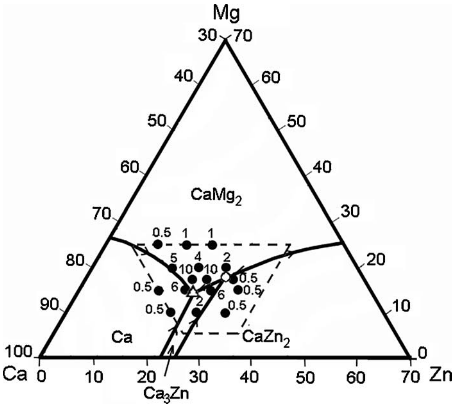

FIG. 1. Liquidus projection of the Ca-Mg-Zn ternary system. The projection shows thick solid lines bounding the Ca, $\mathrm{CaMg}_2$, CaZn, and $\mathrm{Ca}_3\mathrm{Zn}$ phase fields. Ternary eutectic and peritectic compositions are marked by an open triangle and an open circle, respectively. The compositions of amorphous alloys and their maximum plate thicknesses (in mm) are shown as solid circles and pertinent numbers. The trapezoid with a thick dashed boundary represents the composition range for the formation of ternary Ca-Mg-Zn BMGs (Ref. 4).

1098-0121/2010/82(10)/104206(13)

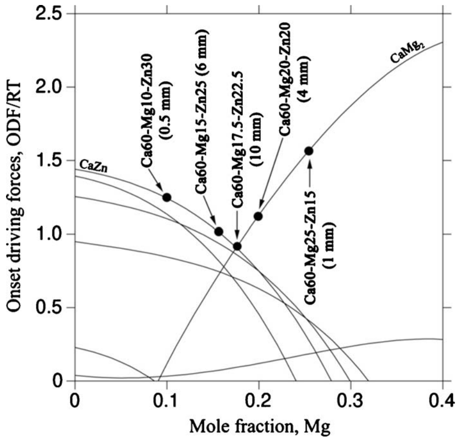

FIG. 2. Calculated onset driving forces of various crystalline phases for $Ca_{60}Mg_XZn_{40-X}$ alloys versus Mg content at 390 K. Two lines corresponding to maximum onset driving forces belong to CaZn and $CaMg_2$ phases. The circles represent the amorphous alloy compositions with indicated critical thicknesses (Ref. 10).

cient solute-centered cluster packing (ECP) model of amorphous structure,[20] the Ca-Mg-Zn ternary glasses are represented as $\langle 10,9 \rangle$ efficient cluster packing structures, where Mg solute atoms are surrounded by approximately ten nearest neighbors and Zn solute atoms have approximately nine nearest neighbors, assuming that all the nearest neighbors are solvent atoms (i.e., Ca). Here, the term *solvent* is used to indicate the atomic species in the glass with the largest atom fraction while the term *solute* denotes the other atomic species in the glass. Glass compositions predicted from the ECP model range from $Ca_{70}Mg_{15}Zn_{15}$ to $Ca_{53}Mg_{12}Zn_{35}$,[21] which fit within the trapezoid shown in Fig. 1. Structural insights from the ECP model have been validated in binary metallic glasses[22] but have not yet been compared with experimental data for ternary metallic glass structures.

It is the objective of the present work to experimentally characterize the local atomic structures in Ca-Mg-Zn ternary metallic glasses. In the following, we use neutron and x-ray diffraction data as the basis on which to model the amorphous structure of a series of ternary $Ca_{60}Mg_XZn_{40-X}$ ($X = 10,15,20,25$ at. %) metallic glasses using Reverse Monte Carlo (RMC) methods. The effect of alloy composition on the structure and GFA is examined and the average amorphous structure identified in this work is compared with the amorphous structure predicted by the ECP model[20] and discussed in comparison with those of other BMG families.

## II. EXPERIMENTAL PROCEDURES

### A. Sample preparation

Four amorphous alloys, $Ca_{60}Mg_{10}Zn_{30}$, $Ca_{60}Mg_{15}Zn_{25}$, $Ca_{60}Mg_{20}Zn_{20}$, and $Ca_{60}Mg_{25}Zn_{15}$, were used in this study. Among these, the $Ca_{60}Mg_{10}Zn_{30}$ and $Ca_{60}Mg_{25}Zn_{15}$ alloys show marginal GFA, with maximum fully amorphous plate thicknesses achievable during water-cooled copper mold casting of 0.5 mm and 1 mm, respectively.[2,4] The two other alloys, $Ca_{60}Mg_{15}Zn_{25}$ and $Ca_{60}Mg_{20}Zn_{20}$ are better bulk glass formers and their maximum fully amorphous plate thicknesses were identified to be 6 mm and 4 mm, respectively. In order to exclude the effects of casting conditions, amorphous specimens of all four alloys were prepared by melt spinning in the form of ~0.2-mm-thick ribbons. The densities, $\rho_o$, of the amorphous alloys were measured with a helium pycnometer AccuPyc 1330 V1.03 and the values (in $g/cm^3$ and atoms/$Å^3$) are given in Table I. The following formula was used for the density conversion:

TABLE I. Density (in $g/cm^3$ and atoms/$Å^3$) of Ca-Mg-Zn amorphous alloys produced in this work.

| | Density | |
|---|---|---|
| Alloy | $g/cm^3$ | Atoms/$Å^3$ |
| $Ca_{60}Mg_{10}Zn_{30}$ | $2.4481 \pm 0.0058$ | 0.031985 |
| $Ca_{60}Mg_{15}Zn_{25}$ | $2.2890 \pm 0.0073$ | 0.031301 |
| $Ca_{60}Mg_{20}Zn_{20}$ | $2.1499 \pm 0.0024$ | 0.030837 |
| $Ca_{60}Mg_{25}Zn_{15}$ | $2.0043 \pm 0.0044$ | 0.030227 |

$$\rho_o \;(\text{atoms}/Å^3) = (N_A / \sum c_i A_i) \rho_o \;(\text{g/cm}^3), \qquad (1)$$

where $N_A$ is the Avogadro's number and $c_i$ and $A_i$ are the atomic fraction and atomic mass, respectively, of the element $i$ (Ca, Mg, or Zn) in a given alloy.

### B. Neutron and x-ray diffraction

Neutron-diffraction experiments were conducted at room temperature under vacuum using the general materials (GEM) diffractometer at the ISIS high-intensity pulsed neutron source (Rutherford Appleton Laboratory, Didcot, U.K.).[23] GEM has eight detector banks which collects data over a wide range in $Q$ (from 0.1 to 100 $Å^{-1}$), where $Q = 4\pi \sin \Theta / \lambda$ is the magnitude of the scattering vector for a neutron of wavelength $\lambda$ scattered at an angle $2\Theta$. The samples were loaded in 10.3 mm diameter cylindrical vanadium cans, and the ribbons were crushed to allow efficient packing of the material. The thickness of the can walls was 25 $\mu$m to minimize corrections. The exposure time for each sample was about 3.5 h. Due to the high degree of structural disorder in these samples, there were no apparent oscillations in the diffraction pattern beyond 25 $Å^{-1}$. X-ray diffraction experiments were conducted at room temperature on a Panalytical Xpert-Pro diffractometer (ISIS Facility) using Ag $K\alpha$ radiation. The samples were powdered and loaded into 1 mm diameter silica capillaries of wall thickness 0.01 mm, which were sealed with wax. The $Q$ range extended from 0.5 to 18 $Å^{-1}$.

ISIS developed software, GUDRUN,[24] GUDRUNX,[25] and ATLAS (Ref. 26) were used to reduce and correct the neutron and x-ray diffraction data. This yields the experimental total scattering structure factors, $S^N(Q)$ and $S^X(Q)$, and the total radial distribution functions (RDFs) $G^N(r)$ for the four studied Ca-Mg-Zn metallic glasses. The superscript $N$ or $X$ indicates that the data was obtained by neutron or x-ray diffraction, respectively. These functions are related to the partial RDFs (PRDFs), $g_{ij}(r)$, by the following equations:[27]

$$S^N(Q) = \frac{4\pi\rho_o}{Q}\sum_{i,j=1}^{3} c_i c_j b_i b_j \int_0^{\infty} r[g_{ij}(r) - 1]\sin(Qr)dr, \quad (2)$$

$$S^X(Q) = \frac{4\pi\rho_o}{Q}\sum_{i,j=1}^{3} c_i c_j \frac{f_i(Q) f_j(Q)}{\sum_{k=1}^{3} c_k f_k(Q)^2} \int_0^{\infty} r[g_{ij}(r) - 1]\sin(Qr)dr, \quad (3)$$

$$G^N(r) = \sum_{i,j=1}^{3} c_i c_j b_i b_j [g_{ij}(r) - 1]. \quad (4)$$

In Eqs. (2)–(4), $c_i$, $b_i$, and $f_i(Q)$ are, respectively, the atomic fraction, coherent bound neutron-scattering length, and x-ray scattering factor of element $i$ (Ca, Mg, or Zn), $\rho_o$ is the average number density of the material (in atoms/Å$^3$), and $r$ is a distance from an average origin atom point in the amorphous structure. The $G^N(r)$ functions for the four studied Ca-Mg-Zn glasses were obtained by Fourier transformation of the respective $S^N(Q)$ functions using the Lorch modification function[28] with a maximum momentum transfer $Q_{\max}$ of 25 Å$^{-1}$.

### C. Reverse Monte Carlo simulation

Three-dimensional models of the amorphous structures of the Ca-Mg-Zn alloys that agree with the experimental data, alloy density and closest approach constraints, were generated with the aid of the RMC simulation technique described in detail in Ref. 29. Simulation boxes with periodic boundary conditions contained 5400 atoms, and the box size was determined by the density of the material being modeled. The input data used in each simulation were the experimental neutron and x-ray total structure factors, $S^N(Q)$ and $S^X(Q)$, and the radial distribution function, $G^N(r)$. $G^X(r)$ was not used because a noticeable error in calculating this function from $S^X(Q)$, determined in a narrow $Q$ range, was expected. Indeed, the $Q$-dependent x-ray scattering factors, $f_i(Q)$, make corrections of $S^X(Q)$ and, especially, $G^X(r)$ from the experimental x-ray data more difficult, and so the results are less reliable, than the neutron data.[30] Use of both $S^N(Q)$ and $G^N(r)$ and only $S^X(Q)$ thus gave more weight to the more reliable neutron data.

The closest approach constraints (i.e., minimum interatomic distances) together with the fixed alloy density have been found to improve the separation of partials in cases where the separation matrix is poorly conditioned.[29,31] These two main constraints were held throughout the whole simulation runs and severely limited the number of structures that were consistent with the experimental data. The minimum pair bond distances, $r_{ij}^{\min}$, between $i$ and $j$ atoms were computed from the results of deconvolution of the first peak of the total correlation function, $T^N(r)$, with Gaussian functions, using a PEAKFIT VERSION 4.12 program (SeaSolve Software, Inc., San Jose, CA),[32]

$$T^N(r) = 4\pi r\rho_o \sum_{i,j=1}^{3} c_i c_j b_i b_j g_{ij}(r)$$
$$= \sum_{i=1}^{3}\sum_{j\leq i}^{3} \frac{a_{ij}}{\sqrt{2\pi}\sigma_{ij}} \exp\left[-\frac{(r - r_{ij})^2}{2\sigma_{ij}^2}\right]. \quad (5)$$

Here, $r_{ij}$ and $\sigma_{ij}$ are, respectively, the most probable (mode) bond distance and the standard deviation of the $i$-$j$ partial (Gaussian) peak, $a_{ij}$ is the peak area, and $r_{ij}^{\min} = r_{ij} - 3\sigma_{ij}$. Thus the following minimum pair-bond distances were applied in the RMC simulations: $r_{\text{Ca-Ca}}^{\min} = 3.26$ Å, $r_{\text{Ca-Mg}}^{\min} = 2.96$ Å, $r_{\text{Ca-Zn}}^{\min} = 2.62$ Å, $r_{\text{Mg-Mg}}^{\min} = 2.58$ Å, $r_{\text{Mg-Zn}}^{\min} = 2.30$ Å, and $r_{\text{Zn-Zn}}^{\min} = 2.17$ Å. (In this paper, we use the term "bond distance" for convenience when discussing two atoms which are nearest neighbors, and this should not be taken as implying that there is any particular type of bonding between the two atoms.) During the initial stages of the RMC simulation, these Gaussian pair-bond distribution profiles were used as additional constraints in order to prevent formation of physically unrealistic structures with sharp peaks of some $g_{ij}(r)$ at $r_{ij}^{\min}$. As soon as a stationary difference between the calculated and experimental RDFs was achieved, these additional constraints were removed and the simulated structure was further refined to achieve the best fit between the experimental and calculated RDFs and total structure factors. More than 10 million accepted random atom moves occurred for each sample before the final configurations were collected, which provided total independence of the modeled structures on the initial configurations of randomly distributed atoms.

The RMC computed amorphous structures were analyzed with the use of freeware programs[33] and programs developed by coauthors from John Hopkins University. These programs allowed the calculation of structural features such as PRDFs; type and distribution of coordination polyhedra (atomic clusters); neighbor coordination numbers (CNs) and triplet angle correlations.

## III. RESULTS

### A. Diffraction data

Figure 3 shows the $G^N(r)$ data for the four samples. Systematic changes with composition can be observed. In particular, the addition of Mg at the expense of Zn results in a decrease in intensity in the region of 2.8–3.3 Å, and an increased intensity between 3.3 and 4.0 Å. Using the metallic and covalent atomic radii[34,35] (Table II) to calculate interatomic distances, it is predicted that the former region is comprised of overlapping correlations from Zn-Zn, Zn-Mg, and Zn-Ca pairs while the latter arises from Mg-Mg, Mg-Ca, and Ca-Ca correlations. The relative change in intensity across the first peak manifold can therefore be understood as relating directly to the exchange of magnesium atoms for zinc in the glass structure. However, information on the precise interatomic distances and coordination numbers of each interatomic pairing cannot be extracted from the data due to the close overlapping of the six individual pair correlations in this system. Such detailed information on the PRDFs can only be extracted by careful modeling of the data.

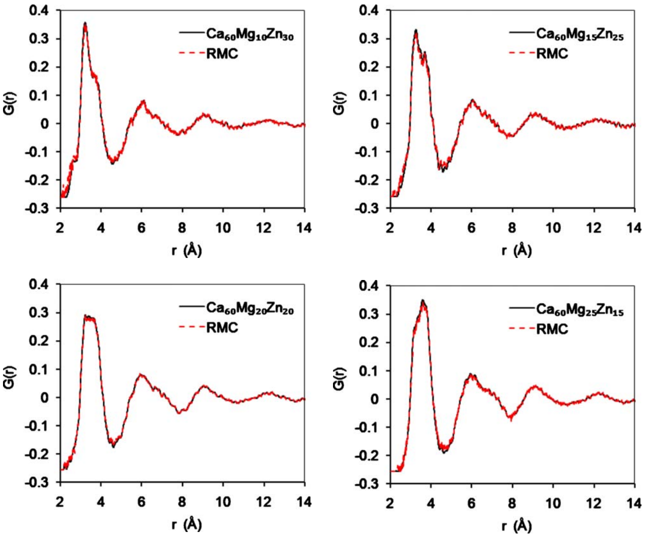

FIG. 3. (Color online) Experimental and RMC simulated neutron total radial distribution functions $G^N(r)$ for $Ca_{60}Mg_XZn_{40-X}$ amorphous alloys.

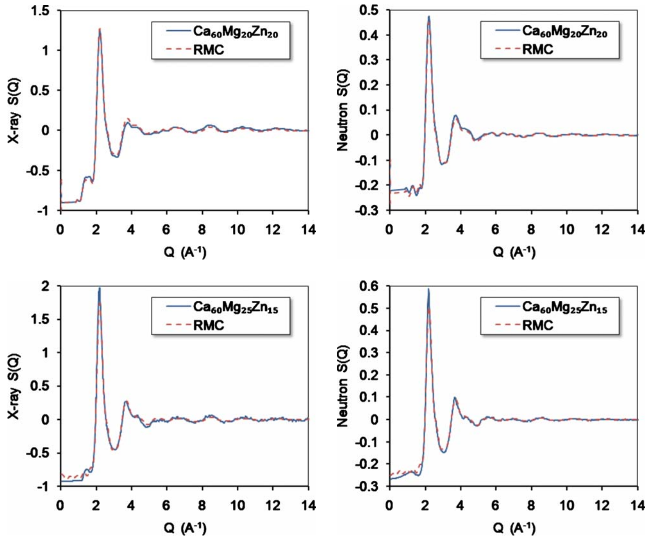

FIG. 4. (Color online) Experimental and RMC simulated x-ray and neutron total scattering structure factors $S(Q)$ for $Ca_{60}Mg_{20}Zn_{20}$ and $Ca_{60}Mg_{25}Zn_{15}$ amorphous alloys.

### B. Pair correlations

The eventual matches between the simulated and experimental $G^N(r)$ for the four Ca-Mg-Zn amorphous alloys, after $\geqslant 10^7$ RMC steps, are shown in Fig. 3 and the total scattering factors are shown for two of the samples in Fig. 4. An excellent fit indicates that the RMC-simulated amorphous structure describes the experimental data very well. The first $G^N(r)$ peak located in the $r$ range between 2.21 and 4.67 Å, corresponds to distances between atoms within the first coordination shell. The six PRDFs for the simulated amorphous structure of $Ca_{60}Mg_{20}Zn_{20}$ are shown in Fig. 5. The PRDFs for the Ca correlations are well determined due to the abundance of Ca in the glass. A single $g_{ij}(r)$ peak inside the first coordination shell range is clearly seen in the Ca-Ca, Ca-Mg, and Ca-Zn PRDFs, and the bond distances, $r_{ij}$, between the Ca-Ca, Ca-Mg, and Ca-Zn pairs corresponding to the maximum of this peak are identified to be 3.84 Å, 3.48 Å, and 3.21 Å, respectively. On the other hand, the Mg-Mg, Mg-Zn, and Zn-Zn correlations are less well defined due to the low abundance of Mg and Zn atoms in this glass system. The first peaks in the PRDFs for these correlations are noisy and rather wide. It is likely that a spectrum of bond distances is typical for the Mg-Mg, Mg-Zn and, especially, Zn-Zn correlations within the first shell (i.e., inside the first RDF peak). A similar behavior of the PRDFs has also been observed for the three other Ca-Mg-Zn amorphous alloys in this study. The interatomic bond distances calculated from the position of the maximum intensity of the first peak of the respective PRDFs for the four Ca-Mg-Zn amorphous alloys are given in Table III.

TABLE II. Metallic, $r_m$, (Ref. 34) and covalent, $r_c$, (Ref. 35) bond distances (in Å) between Ca, Mg, and Zn atom pairs.

| | Ca-Ca | Ca-Mg | Ca-Zn | Mg-Mg | Mg-Zn | Zn-Zn |
|---|---|---|---|---|---|---|
| $r_m$ (Å) | 3.94 | 3.57 | 3.31 | 3.20 | 2.94 | 2.68 |
| $r_c$ (Å) | 3.52 | 3.17 | 2.98 | 2.82 | 2.63 | 2.44 |

Coordination number weighted bond distances, $r_{ij}^{weighted}$, between atom pairs within the first peak of the total RDFs of the Ca-Mg-Zn amorphous alloys are given in Table IV. They are calculated using the following equation:

$$r_{ij}^{weighted} = \int_{r_1}^{r_2} r g_{ij}(r) dr \Bigg/ \int_{r_1}^{r_2} g_{ij}(r) dr, \tag{6}$$

where $r_1$ and $r_2$ are the minimum and maximum cutoffs for the first shell. When the values in Table IV are compared with respective values in Table III, it is found that $r_{ij}^{weighted}$ are always higher than the $r_{ij}$ values at the first peak maximum intensity. The difference increases with a decrease in the size of pair atoms. This finding indicates that the $g_{ij}(r)$ peaks are asymmetrical (non-Gaussian), especially for the Mg-Mg, Mg-Zn, and Zn-Zn atom pairs, which is an indication that these pairs have a wide spectrum of bond distances within the first shell.

## IV. DISCUSSION

### A. Pair correlations

The interatomic bond distances calculated from the position of the maximum intensity of the first peak of the respective PRDFs for the four Ca-Mg-Zn amorphous alloys (Table III) are about 2.3–4.1 % smaller than the respective metallic bond distances, $r_m$, and about 6.5–9.8 % larger than the respective covalent bond distances, $r_c$ (see Table II). The Ca-Zn bonds are noticeably shorter and Zn-Zn bonds are longer in marginal glasses ($Ca_{60}Mg_{10}Zn_{30}$ and $Ca_{60}Mg_{25}Zn_{15}$) than in bulk glass formers ($Ca_{60}Mg_{15}Zn_{25}$ and $Ca_{60}Mg_{20}Zn_{20}$). Table V provides characteristic first-shell bond distances between Ca, Mg, and Zn atom pairs in several crystalline binary intermetallics.[36] There are discrete

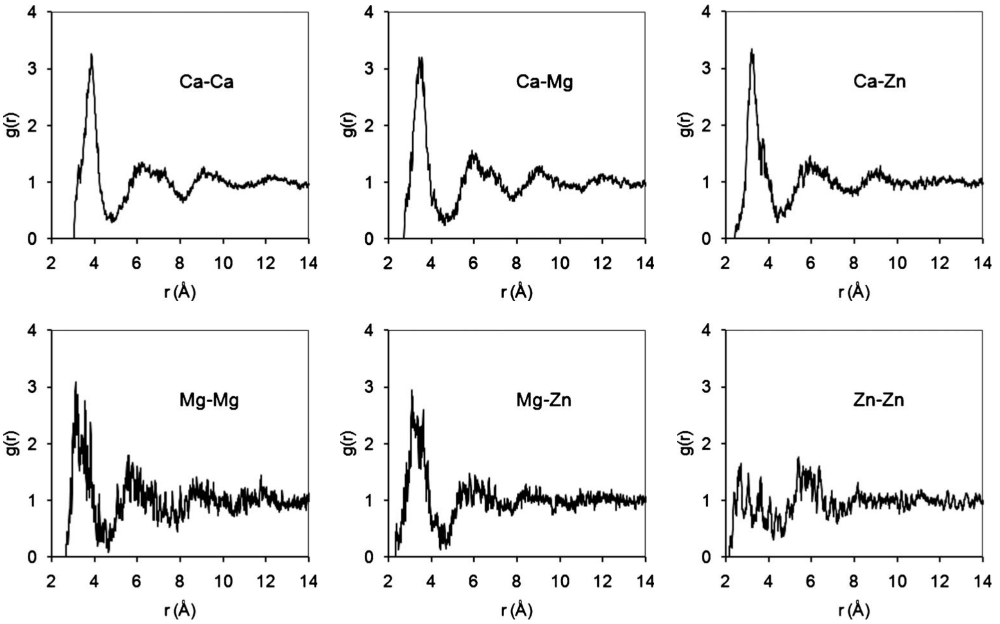

FIG. 5. RMC-simulated partial radial distribution functions $g_{ij}(r)$ for Ca-Ca, Ca-Mg, Ca-Zn, Mg-Mg, Mg-Zn, and Zn-Zn atomic pairs in $Ca_{60}Mg_{20}Zn_{20}$ amorphous alloy.

values of the bond distances constrained by long-range order of a crystal structure in these intermetallics. The minimum bond distances between Ca-Ca, Ca-Zn, Mg-Mg, and Zn-Zn pairs in the intermetallic phases are smaller while those between Ca-Mg and Zn-Mg pairs are larger, than the lengths of respective metallic bonds (compare the data in Tables II and V) indicating presence of covalent components in these crystal structures. The peak Ca-Mg and Zn-Mg pair distances in the amorphous Ca-Mg-Zn alloys given in Table III are smaller than the minimum distances between respective pairs in the crystalline intermetallic phases while the peak $r_{ij}$ values for other four pairs in the amorphous alloys are close to the minimum $r_{ij}$ values in the crystalline intermetallics. This comparative analysis indicates that the absence of long-range order constraints allows shortening of interatomic distances between the nearest neighbor atoms in the amorphous structure, as compared to the binary intermetallics and pure metals.

The observation that some nearest-neighbor bond lengths are shorter than those in the competing long-range ordered crystals may help explain why these glasses are easy glass formers. The equilibrium crystalline phases that compete with the amorphous phase appear to minimize total energy by sacrificing optimal short-range order to achieve beneficial long-range order. The absence of long-range atomic order is an energetic disadvantage but allows metallic glasses to maintain optimized short-range atomic interactions that help reduce the energy difference between the metastable glass and equilibrium crystal(s). The largest contribution to the stability of condensed phases is expected to come from nearest-neighbor interactions so that the optimized short-range interactions in metallic glasses can produce structures that have only a small energetic disadvantage relative to the equilibrium structure. Kinetic constraints from quenching restrict the long-range atomic redistribution needed to achieve long-range order and to further minimize the total system

TABLE III. The interatomic bond distances ($r_{ij}$, in Å), that correspond to the position of the maximum intensity of the first peak in the respective PRDFs of $Ca_{60}Mg_XZn_{40-X}$ amorphous alloys. The bond distance values averaged for the four alloys, $(r_{ij})_{\mathrm{aver}}$, as well as the deviations of these values from metallic, $r_m$, and covalent, $r_c$, bond distances (see Table II), are also given here.

| $r_{ij}$ (Å) | $r_{\mathrm{Ca\text{-}Ca}}$ | $r_{\mathrm{Ca\text{-}Mg}}$ | $r_{\mathrm{Ca\text{-}Zn}}$ | $r_{\mathrm{Mg\text{-}Mg}}$ | $r_{\mathrm{Mg\text{-}Zn}}$ | $r_{\mathrm{Zn\text{-}Zn}}$ |
|---|---|---|---|---|---|---|
| $Ca_{60}Mg_{10}Zn_{30}$ | 3.82 | 3.44 | 3.14 | 3.02 | 2.84 | 2.66 |
| $Ca_{60}Mg_{15}Zn_{25}$ | 3.80 | 3.48 | 3.19 | 3.06 | 2.78 | 2.56 |
| $Ca_{60}Mg_{20}Zn_{20}$ | 3.84 | 3.48 | 3.21 | 3.02 | 2.84 | 2.56 |
| $Ca_{60}Mg_{25}Zn_{15}$ | 3.81 | 3.52 | 3.16 | 3.09 | 2.85 | 2.63 |
| $(r_{ij})_{\mathrm{aver}}$ | 3.82 | 3.48 | 3.18 | 3.05 | 2.87 | 2.60 |
| $100\%(r_{aver}/r_m-1)$ | −3.1 | −2.5 | −4.1 | −4.8 | −2.3 | −2.9 |
| $100\%(r_{aver}/r_c-1)$ | 8.5 | 9.8 | 6.5 | 8.1 | 9.2 | 6.7 |

TABLE IV. Weighted bond distances, $r_{ij}^{weighted}$ (in Å), between the atom pairs within the first global peak of the corresponding PRDFs of the $Ca_{60}Mg_XZn_{40-X}$ amorphous alloys [Eq. (6)]. The weighted bond distance values averaged for the four alloys, $(r_{ij}^{weighted})_{aver}$, as well as the difference between $(r_{ij}^{weighted})_{aver}$ and $(r_{ij})_{aver}$, (taken from Table III) are also given.

| $r_{ij}^{weighted}$ (Å) | Ca-Ca | Ca-Mg | Ca-Zn | Mg-Mg | Mg-Zn | Zn-Zn |
|---|---|---|---|---|---|---|
| $Ca_{60}Mg_{10}Zn_{30}$ | 3.83 | 3.55 | 3.32 | 3.35 | 3.20 | 3.21 |
| $Ca_{60}Mg_{15}Zn_{25}$ | 3.85 | 3.57 | 3.29 | 3.40 | 3.33 | 3.30 |
| $Ca_{60}Mg_{20}Zn_{20}$ | 3.85 | 3.53 | 3.35 | 3.44 | 3.34 | 3.36 |
| $Ca_{60}Mg_{25}Zn_{15}$ | 3.85 | 3.52 | 3.43 | 3.43 | 3.19 | 3.38 |
| $(r_{ij}^{weighted})_{aver}$ | 3.84 | 3.54 | 3.35 | 3.40 | 3.26 | 3.31 |
| $(r_{ij}^{weighted})_{aver}-(r_{ij})_{aver}$ | 0.02 | 0.06 | 0.17 | 0.35 | 0.39 | 0.71 |

energy, thus favoring glass formation. The present results suggest that metallic glasses not only have SRO but may have "better" short-range topological order (in terms of optimal bond length and/or atomic arrangement) than the competing crystals.

The Ca-Mg-Zn amorphous structures show asymmetrical (non-Gaussian) distribution of the neighbor bond lengths, which result in weighted (i.e., mean) bond distances, $r_{ij}^{weighted}$, between the atom pairs to be always higher than the most probable (i.e., mode) pair distances, $r_{ij}$, that correspond to the position of the first peak maximum intensity in the respective PRDFs (see Tables III and IV). The difference between $r_{ij}^{weighted}$ and $r_{ij}$ is minimum for Ca-Ca pairs (~0.02 Å), increases in the order of Ca-Mg, Ca-Zn, Mg-Mg, Mg-Zn, and is maximum for Zn-Zn pairs (~0.71 Å). The clearly identified and more symmetrical PRDF peaks for the Ca-Ca, Ca-Mg, and Ca-Zn atom pairs within the first coordination shell, with the mean and mode interatomic distances equal to or shorter than the neighbor bond distances found in crystalline metals, may suggest that the atoms in these pairs attract and are touching each other. On the other hand, the highly asymmetrical distributions of the bond distances for the Mg-Mg, Mg-Zn, and Zn-Zn atom pairs is an indication that these pairs have a spectrum of bond distances within the first shell. Although some of these pairs are close packed and their mode pair distances are shorter, their mean distances are much longer than the respective metallic bond distances (compare Tables II–IV), indicating that Mg and Zn are less attractive to each other than to Ca. Based on these results, one can suggest that, in average, Mg- and Zn-centered clusters prefer to have Ca atoms as nearest neighbors, while Mg and Zn atoms in the first shell just fill the gaps between the Ca atoms, so that their distances from the center atom (Mg or Zn) vary depending on the gap sizes. These observations also suggest that pairs of Zn atoms more strongly prefer to be separated than other atom pairs.

TABLE V. Characteristic bond distances for coordination polyhedra in several crystalline binary intermetallic phases (Ref. 36).

| $r$ (Å) | $r_{Ca\text{-}Ca}$ | $r_{Ca\text{-}Mg}$ | $r_{Ca\text{-}Zn}$ | $r_{Mg\text{-}Mg}$ | $r_{Mg\text{-}Zn}$ | $r_{Zn\text{-}Zn}$ |
|---|---|---|---|---|---|---|
| $CaMg_2$ | 3.81 | 3.62 | | 3.05 | | |
| | | | | 3.13 | | |
| | | | | 3.18 | | |
| $Ca_3Zn$ | 3.78 | | 3.18 | | | 4.15 |
| | 3.88 | | 3.56 | | | |
| | 3.91 | | 4.17 | | | |
| | 3.95 | | | | | |
| | 4.15 | | | | | |
| | 4.32 | | | | | |
| CaZn | 3.90 | | 3.18 | | | 2.62 |
| | 4.05 | | 3.22 | | | |
| | 4.20 | | | | | |
| $MgZn_2$ | | | | 3.17 | 3.04 | 2.53 |
| | | | | | | 2.61 |
| | | | | | | 2.64 |
| $Ca_5Zn_3$ | 3.61 | | 3.14 | | | 2.69 |
| | 3.76 | | 3.29 | | | |
| | 4.07 | | 3.34 | | | |
| | 4.19 | | | | | |
| Minimum | 3.61 | 3.62 | 3.14 | 3.05 | 3.04 | 2.53 |
| Maximum | 4.32 | 3.62 | 4.17 | 3.18 | 3.04 | 4.15 |

### B. Coordination polyhedra

Atoms in metallic glasses tend to arrange themselves so as to maximize the local packing density[20,37–39] and the finite sizes of atoms impose geometrical restrictions on the possible local atom environments.[40,41] The local environment of an atom is generally treated in terms of the geometry of the shell formed by its nearest-neighbor atoms.[42,43] The chemistry (i.e., the number of different atom species and their relative positions) of the first coordination shell provides additional important information about the local environment. Bonding in metallic glasses is generally nondirectional, and the nearest neighbors for any chosen atom *i* are often defined as those atoms that are either in contact with *i*, or separated from it by a distance smaller than a certain threshold value. The latter is defined globally as the position of the first minimum of the RDF of the whole atomic array. Therefore, this approach is not sensitive to the details of the first shell geometry and/or to local density and chemistry fluctuations.

A more advanced approach is to define the nearest neighbors as atoms that have common faces in their Voronoi polyhedra.[37] This definition of the first coordination shell atoms is straightforward and reflects local details of the atomic packing topology. In this approach, a *coordination polyhedron* with vertices located in positions of the first coordination shell atoms and with edges coinciding with the interatomic bonds is defined for any chosen atom $i$.[43] Each coordination polyhedron, which is also called an $i$-centered cluster,[15,20] is associated with the respective $i$-centered Voronoi polyhedron and can therefore be assigned the characteristic Voronoi signature $(v_3,v_4,v_5,v_6)$. For the Voronoi polyhedron, $v_m$ is the number of faces containing $m$ edges while for the respective coordination polyhedron, $v_m$ is the number of the vertices common to $m$ polyhedron edges (or faces).[44] In the latter case, $m$ is also called the vertex coordination. The bond connecting the center atom $i$ with an $m$-coordinated neighbor atom/vertex $j$ is perpendicular to an $m$-edged face in the respective $i$-centered Voronoi polyhedron, and thus called an $m$-fold bond. Those $i$-centered clusters with the same Voronoi signature are considered to be topologically equivalent (even though they may not be identical) because they can be transformed into each other by 'elastic' deformation without changing the number of vertices and connecting edges. In addition to assigning topology, the Voronoi signature also defines the total CN of the cluster as $\mathrm{CN}=\Sigma v_m$. Clusters with the same Voronoi signature can however be chemically different if they consist of different elements. Therefore, in addition to the Voronoi signature, partial coordination numbers, i.e., the number of atoms of different species, should also be known for a more complete description of the SRO in the amorphous structure.

Figure 6 illustrates the types and fractions of Ca-, Mg- and Zn-centered coordination polyhedra found in the RMC-simulated amorphous structures of the four Ca-Mg-Zn alloys. Although many types of coordination polyhedra are present in the amorphous structures, the most common clusters can be identified. These are (0,1,10,2) for Ca-centered, (0,2,8,1) for Mg-centered, and (0,3,6,0), (0,2,8,1), (0,3,6,1), and (0,2,8,0) for Zn-centered clusters. Three examples of the clusters extracted from the amorphous structures are illustrated in Fig. 7. The characteristic coordination polyhedra in all these Ca-Mg-Zn glasses are not dominated by (0,0,12,0) icosahedra and Mg- and Zn-centered polyhedra with CNs of 11, 10, and 9 are actually more common. This is similar to the Cu-Zr BMGs on the Zr-rich side, where solute Cu atoms are surrounded mostly by solvent Zr and have CNs lower than 12, but different from the more Cu-rich Cu-Zr (and Cu-Zr-Al) BMGs, where the Cu-centered (0,0,12,0) icosahedra with both Cu and Zr in the shell are the dominant structural unit influencing the GFA and properties.[11–13]

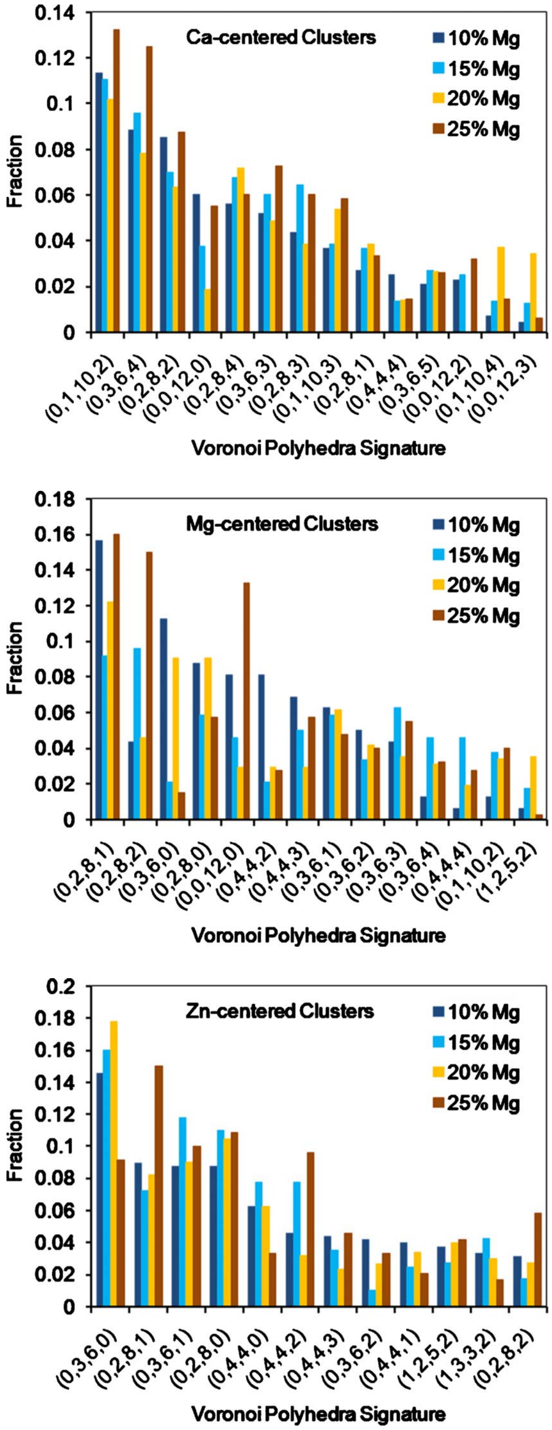

FIG. 6. (Color online) Types of Ca-, Mg-, and Zn-centered clusters and their fractions in four $\mathrm{Ca}_{60}\mathrm{Mg}_X\mathrm{Zn}_{40-X}$ amorphous alloys.

Whereas the simulated amorphous structures of $\mathrm{Ca}_{60}\mathrm{Mg}_X\mathrm{Zn}_{40-X}$ alloys contain many types of coordination polyhedra, the competing crystal phases, $\mathrm{CaMg}_2$ and CaZn,[10] contain only three and two types of polyhedra, respectively.[36] Figure 8 shows the three principal clusters (one is Ca-centered and two are Mg-centered) that are present in the $\mathrm{CaMg}_2$ intermetallic phase, and Fig. 9 shows the two clusters (Ca- and Zn-centered, respectively) found in the CaZn intermetallic phase. The Ca-centered clusters, (0,0,12,4) in $\mathrm{CaMg}_2$ and (0,1,10,6) in CaZn, are not present in the analyzed amorphous structures where the number of atoms around each Ca atom is found to be significantly less than 16–17, indicating that the local environment of Ca is not efficiently packed in the amorphous structure. Both Mg-centered clusters in $\mathrm{CaMg}_2$ are of the (0,0,12,0) type and the Zn-centered cluster in CaZn is (0,3,6,0). Similar Mg- and Zn-centered clusters are also common in the amorphous structures (see Fig. 6). This is different from transition metal

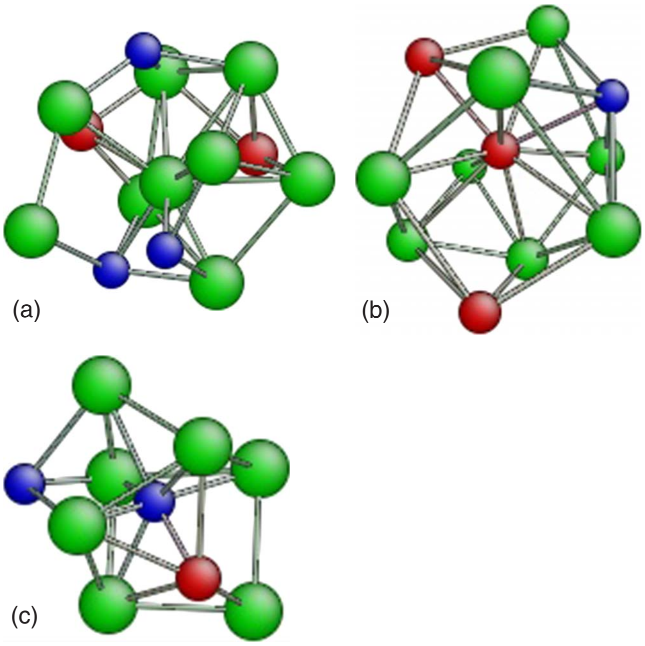

FIG. 7. (Color online) Configurations of three typical (a) Ca-centered (0,1,10,2), (b) Mg-centered (0,2,8,1), and (c) Zn-centered (0,3,6,1) clusters in the $Ca_{60}Mg_XZn_{40-X}$ amorphous alloys.

Zr-Cu glasses, where the dominant icosahedra and related clusters are not found in the competing crystalline compounds.

Of particular note is the increase in the fraction of (0,0,12,0) Mg clusters from ~0.03 to ~0.13 when the Mg content is increased from 20 to 25 at. %. This increase results in the cluster being the third most common in the glass, with the fraction of the two most common clusters, (0,2,8,1) and (0,2,8,2), also increasing significantly over this compositional range. Furthermore, in contrast to the other clusters found in the models, these latter two clusters are 11 or 12 coordinated and have more than two thirds of the vertices with the coordination number $m=5$, making them most like the (0,0,12,0) icosahedral cluster. This tendency toward 12-coordinated Mg and $m=5$ coincides with a reduction in the maximum amorphous thickness from 4 to 1 mm, and the formation of $CaMg_2$. While less obvious, there is a similar increase in the number of Ca atoms with coordination numbers of 12 and 13 and a predominance of $v_5$, with the three most dominant clusters for the $Ca_{60}Mg_{25}Zn_{15}$ glass being (0,1,10,2), (0,3,6,4) and (0,2,8,2), all of which, in addition to (0,0,12,0), are present in significantly higher amounts than in the $Ca_{60}Mg_{20}Zn_{30}$ glass. No such trends toward CaZn-like clusters can be seen in the Zn environments but the fraction of "favorable" (0,3,6,0) clusters is found to reduce dramatically as the Mg content increases from 20 to 25 at. %, and $CaMg_2$ is formed in preference to CaZn. Therefore, increases in the fraction of local clusters that are topologically similar to crystalline compounds can be correlated with the reduction in GFA but their presence does not negate glass formation. This is true for oxide glasses such as amorphous $SiO_2$ and for the binary Pd-Si BMG,[45] and the BMG-forming Ca-Mg-Zn case shows that it is also true for more complex metallic glasses.

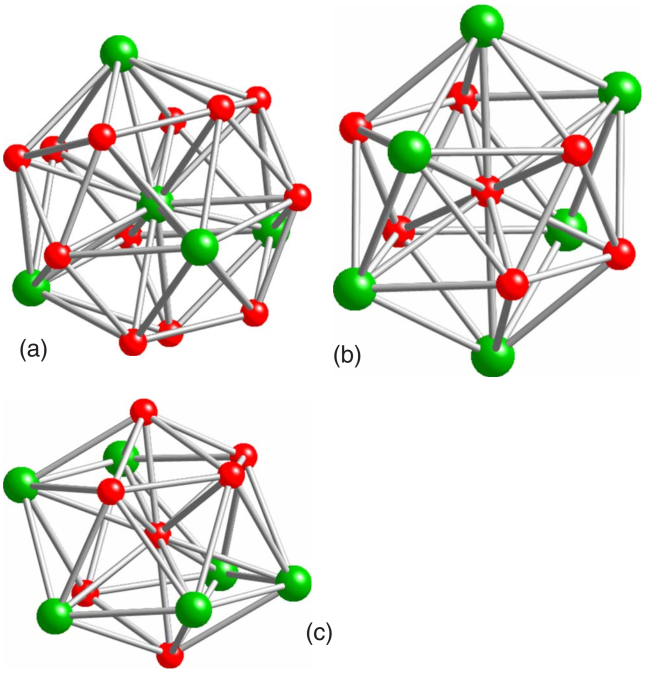

FIG. 8. (Color online) (a) Ca-centered (0,0,12,4) and (b) and (c) Mg-centered, both are (0,0,12,0), coordination polyhedra in the $CaMg_2$ crystal structure (Ref. 36).

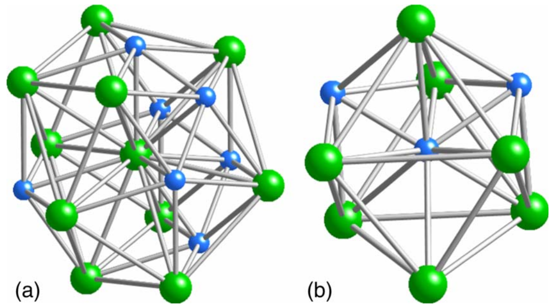

FIG. 9. (Color online) (a) Ca-centered (0,1,10,6) and (b) Zn-centered (0,3,6,0) coordination polyhedra in the CaZn crystal structure (Ref. 36).

### C. Coordination numbers

The distributions of the atomic clusters by the total CN in the first shell are shown in Fig. 10. There is no notable difference in the distributions between good ($X=15$ and 20) and marginal ($X=10$ and 25) glass formers. The most common coordination numbers are CN=13 for the Ca-centered clusters, CN=11 and 12 for Mg-centered clusters and CN=10 for Zn-centered clusters.

Figure 11 shows the average number of Ca, Mg, and Zn atoms in the first shell of the Ca-, Mg-, and Zn-centered clusters in the Ca-Mg-Zn amorphous alloys. Ca atoms are most common in the first shell of the clusters and an increase in the concentration of Mg from 10% to 25% almost does not affect the number of Ca atoms in all three types of clusters. The respective Ca-Ca, Mg-Ca, and Zn-Ca partial coordination numbers (PCNs) are $n_{\text{Ca-Ca}}=8.1-8.5$, $n_{\text{Mg-Ca}}=7.2-7.9$,

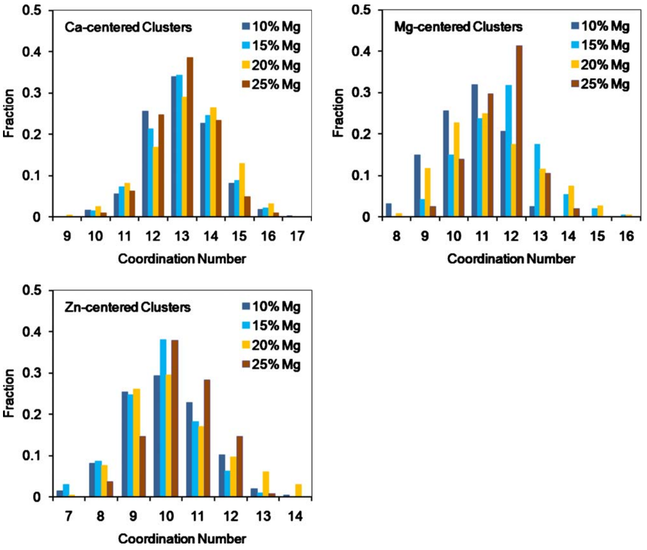

FIG. 10. (Color online) Distributions of Ca-centered, Mg-cantered, and Zn-centered clusters by their total coordination numbers in four $Ca_{60}Mg_XZn_{40-X}$ amorphous alloys.

and $n_{\text{Zn-Ca}}=6.7-7.2$. In comparison, an increase in the concentration of Mg does result in an increase in the number of Mg atom neighbors (i.e., $n_{\text{Ca-Mg}}$ increases from 1.2 to 3.0 and $n_{\text{Mg-Mg}}$ increases from 0.9 to 3.7) and a corresponding decrease in the number of Zn atom neighbors ($n_{\text{Ca-Zn}}$ decreases from 3.3 to 1.8 and $n_{\text{Mg-Zn}}$ decreases from 2.3 to 0.6) in the Ca- and Mg-centered clusters. The number of Zn and Mg atoms in the first shell of Zn-centered clusters does not vary linearly and a link between the GFA and the local environments can be made. Namely, marginal glasses (with 10% and 25% Mg) have more Zn and less Mg in the first shell of the Zn-centered clusters than good glass-forming alloys (with 15% and 20% Mg).

The CN values for the Zn- and Mg-centered clusters are higher than the CN values of 9 and 10, expected for these clusters from the solute-centered ECP model.[20] However, the ECP model assumes that only solvent (Ca) atoms are present in the first coordination shell. If some Ca atoms are replaced by the smaller Mg and Zn atoms, a larger number of atoms can be expected in the first shell. This idea is explored quantitatively by calculating the packing efficiency around Ca, Mg, and Zn atoms. Using the partial coordination numbers in Fig. 11, atomic radii in Table III and the analytic approach in Ref. 38 the following results are found. Packing around Mg atoms ranges from 96% for $Ca_{60}Mg_{10}Zn_{30}$ to 103% for $Ca_{60}Mg_{15}Zn_{25}$ and $Ca_{60}Mg_{20}Zn_{20}$. Within an anticipated accuracy of ±10%, these results show that all of the available space in the first coordination shell of Mg atoms is fully occupied by the combination of Ca, Mg, and Zn atoms indicated in Fig. 11. The packing efficiency around Zn atoms is similarly efficient and ranges from 103% for $Ca_{60}Mg_{10}Zn_{30}$ to 109% for $Ca_{60}Mg_{20}Zn_{20}$ and $Ca_{60}Mg_{25}Zn_{15}$. However, the packing around Ca atoms ranges from 87–88 % and does not reaches maximum packing efficiency. This result for Ca-Mg-Zn glasses is similar to the results for an $Al_{87}Y_8Ni_5$ glass,[38] where packing around Y and Ni solutes was within 100±10% and packing around the solvent (Al) atoms was only 69%. A notable difference is that packing around Ca solvent atoms in the Ca-Mg-Zn BMGs is significantly higher than packing around the Al solvents in the marginal $Al_{87}Y_8Ni_5$ glass, suggesting that the more efficient packing of solvent atoms around Ca contributes to the higher GFA relative to the Al-Y-Ni glass.

A local packing efficiency that exceeds 100% around Mg- and Zn-centered clusters is consistent with the broad range of Zn-Zn, Zn-Mg, and Mg-Mg interatomic separations in the first shell. Specifically, the packing efficiency reported in the preceding paragraph was estimated under the assumption that the first shell atoms are in contact with the central atom. To reduce compression strains associated with "overpopulation" in the first coordination shell, some Mg and Zn atoms occupy positions farther from the central atom. This gives a wider and less symmetrical first PRDF peak for Mg-Mg, Mg-Zn, and Zn-Zn pairs. As a result, the differences between the pair distances corresponding to the maximum peak intensity (mode) and weighted average (median) become large (see Tables III and IV). On the other hand, for Ca-centered clusters, where the local packing efficiency was found to be ~87–88 %, all the first shell atoms contact the surface of the central Ca atom. As a result, a very sharp first peak on the corresponding Ca-Me PRDFs (Me represents Ca, Mg, or Zn) is observed. Moreover, the peak and weighted distances for the Ca-Me pairs have almost the same values.

As it has been mentioned earlier, the neighbor environment of a specific $j$ atom in the first coordination shell of an $i$-centered cluster can be described by the vertex coordination number $m_j$, i.e., the number of neighbors of the $j$ atom located in the first shell of the $i$-centered cluster[39,43] or the number of edges (bonds) entering the vertex $j$. Figure 12 shows the fraction of 3-, 4-, 5- and 6- coordinated vertices in the Ca-, Mg-, and Zn-centered clusters. In all three cluster types, the vertex coordination $m=5$ prevails. The dominance of polyhedra with 4-, 5-, and 6-bond vertices has been shown[42,43] to be an indication of dense atomic packing of the amorphous structure. Moreover, a high fraction of 5-bond

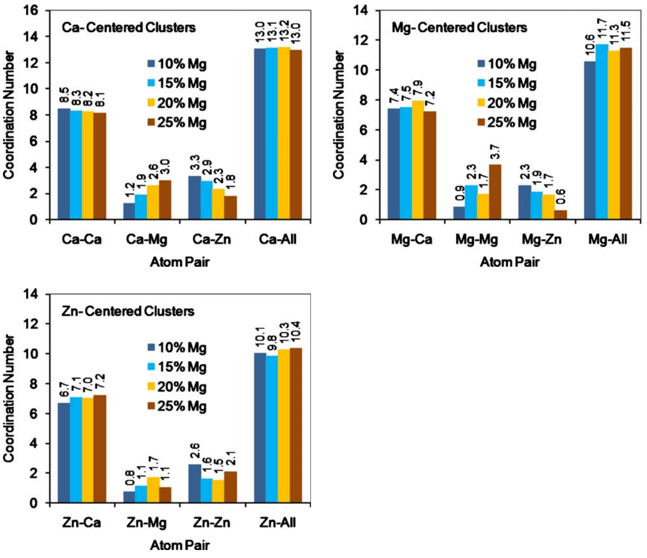

FIG. 11. (Color online) Partial coordination numbers in $Ca_{60}Mg_XZn_{40-X}$ amorphous alloys as a function of Mg content.

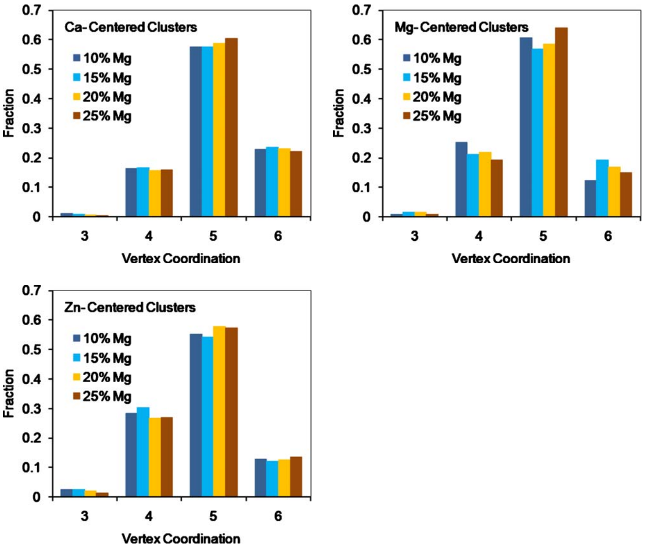

FIG. 12. (Color online) Fraction of vertices with 3, 4, 5, and 6 neighbor atoms (bonds) in Ca-, Mg-, and Zn-centered clusters in four $Ca_{60}Mg_XZn_{40-X}$ amorphous alloys.

vertices can indicate dominance of pentagonal bipyramids as structural units in the amorphous structure. Two pentagonal bipyramids with a common fivefold vertex connected by ten tetrahedra with common faces form a coordination icosahedron, which is believed to be the most common cluster in some important BMGs, such as Cu-rich Cu-Zr.[46] In Ca-Mg-Zn, however, many of the pentagonal bipyramids do not form complete (0,0,12,0) icosahedra. This is clearly indicated by inspection of the Voronoi signatures, $(v_3, v_4, v_5, v_6)$, in Fig. 6, which shows that none of the values of $v_3$, $v_4$, or $v_6$ are larger than $v_5$, regardless of the value of the CN. This is also indicated by the low fraction of clusters with the (0,0,12,0) Voronoi index.

### D. Bond-angle distributions

Bond angle distributions can provide additional information about the most common local structures around cluster vertices because characteristic vertex angles are very sensitive to the vertex type (e.g., number and length distributions of vertex bonds). Figure 13 shows Ca-Ca-Ca, Ca-Mg-Ca, and Ca-Zn-Ca bond angle distributions in the Ca-Mg-Zn amorphous structures. The upper limit of the bond lengths has been set to 4.6 Å, which corresponds to the minimum after the first peak of the total RDFs. A characteristic feature for all four alloys is the first peak located near 60°. The exact 60° angle position for the Ca-Ca-Ca triplets corresponds to the close packing of three equal hard spheres, forming equilateral triangles [Fig. 13(d)]. For the Mg- and Zn-centered triplets (i.e., Ca-Mg-Ca and Ca-Zn-Ca), the first peak is located at $\sim 64°$ and $\sim 68°$, respectively. These shifts of the first peak angle to higher values can be explained by the smaller atomic radii of Mg and Zn atoms. From the known bond angle values, the most common bond distance ratios are estimated to be $r_{\text{Ca-Mg}}/r_{\text{Ca-Ca}}=0.94$ and $r_{\text{Ca-Zn}}/r_{\text{Ca-Ca}}=0.89$, which leads to the effective atomic radius ratios of $(r_{\text{Mg}}/r_{\text{Ca}})_{\text{eff}}=0.88$ and $(r_{\text{Zn}}/r_{\text{Ca}})_{\text{eff}}=0.78$. These calculated radius ratios are higher than both the metallic, $(r_{\text{Mg}}/r_{\text{Ca}})_m=0.81$ and $(r_{\text{Zn}}/r_{\text{Ca}})_m=0.68$, and the covalent radius ratios, $(r_{\text{Mg}}/r_{\text{Ca}})_c=0.80$ and $(r_{\text{Zn}}/r_{\text{Ca}})_c=0.69$, calculated from Table II. The observed Ca-Mg-Ca and Ca-Zn-Ca triplet configurations can be explained by larger shortening of Ca-Ca bonds than Ca-Mg and Ca-Zn bonds (relative to the respective metallic bond distances), which is in agreement with the weighted bond distance data reported in Table IV.

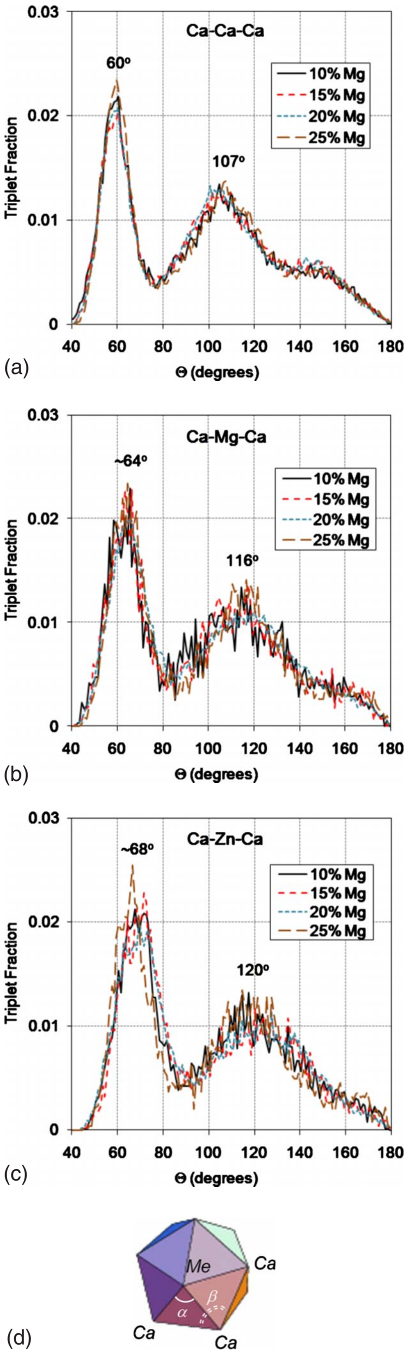

FIG. 13. (Color online) (a) Ca-Ca-Ca, (b) Ca-Mg-Ca, and (c) Ca-Zn-Ca bond-angle distributions in $Ca_{60}Mg_XZn_{40-X}$ amorphous alloys. A pentagonal pyramid with two characteristic peak bond angles, $\alpha \sim 60°-67°$ and $\beta \sim 107°-120°$, is shown in (d) and represents the most common configuration in the first coordination shell. *Me* in figure (d) represents Ca, Mg, or Zn.

TABLE VI. Structural parameters of $Ca_{60}Mg_{15}Zn_{25}$ obtained from *ab initio* MD simulation.

| Center | Neighbor | Average bond length (Å) | Partial CN | Total CN |
|---|---|---|---|---|
| Ca | Ca | 3.8 | 8.7 | 13.7 |
| | Mg | 3.5 | 2.0 | |
| | Zn | 3.2 | 3.0 | |
| Mg | Ca | 3.5 | 8.0 | 11.5 |
| | Mg | 3.2 | 1.3 | |
| | Zn | 2.9 | 2.2 | |
| Zn | Ca | 3.2 | 7.3 | 9.3 |
| | Mg | 2.9 | 1.3 | |
| | Zn | 2.6 | 0.7 | |

The second bond-angle distribution peak, which is located near 107° for Ca-Ca-Ca triplets, corresponds to the interior angle of 108° of a regular pentagon [see Fig. 13(d), angle $\beta$]. A slightly smaller value is probably due to slight distortion of the pentagon, when one of the five Ca atoms in the pentagon vertices is replaced by Mg and/or Zn. Due to the shorter Ca-Mg (or Ca-Zn) bonds, the interior angle at the Mg (Zn) vertex of the pentagon increases at the expense of other interior angles, the total sum of which is 540° in the pentagon. Indeed, the second peak for Ca-Mg-Ca and Ca-Zn-Ca triplets is located at ~116° and ~120°, respectively. Having a pentagon consisting of four Ca atoms and one Mg/Zn atom and using these values of the interior angle at the Mg/Zn vertex, the interior angles at the other four Ca vertices are calculated to be 106°/105°. To obtain the average angle of 107° for the Ca-Ca-Ca triplets, it should be assumed that one Mg/Zn atom replaces every 10th/15th Ca atom in the pentagon configurations present in the amorphous structure.

The two characteristic peaks in the bond-angle distributions correspond to the angles at the vertices of equilateral triangles and pentagons and support our earlier conclusion that tetrahedra and pentagonal bipyramids are the most common atomic configurations in the $Ca_{60}Mg_XZn_{40-X}$ amorphous alloys.

### E. *Ab initio* molecular-dynamics simulation

To investigate whether the structure obtained using RMC is physically stable and favored, we have performed *ab initio* molecular-dynamics (MD) simulation for the representative composition $Ca_{60}Mg_{15}Zn_{25}$. The cubic supercell with 200 atoms and periodic boundary condition was equilibrated at 1000 K for 100 ps, and quenched to 300 K at ~10 K/ps, using VASP.[47]The box size was chosen to correspond to the experimental density. The final configuration at 300 K was analyzed using the same program and parameters, and the main structural features are in agreement with the RMC results; see Table VI for the bond length and the CNs. The fraction of fivefold bonds is also dominant (~60%).

### F. Structural description via efficient cluster packing

Structural descriptions using the ECP model have recently been established for binary metallic glasses[20] but extension to ternary glasses has not yet been accomplished. As a result, only general consistency between the ECP model and the present results are possible. The most significant finding of the present research that validates the underlying physical principle of the ECP model is the formation of a structural scaffold consisting of efficiently packed solute-centered clusters surrounded primarily by Ca atoms. Earlier concepts suggest that the largest solute dominates the structure by forming the solute-centered clusters which form the structural scaffold.[18,20] The relative size between the $\alpha$ solute and the solvent defines the number of solvent sites that surround each $\alpha$ site, and smaller solutes fit in $\beta$ and $\gamma$ sites situated at the center of octahedra and tetrahedra of the primary clusters, respectively. Although the largest solute has been assumed to occupy $\alpha$ sites based on its topological potency (it bonds to more solvent atoms than smaller solutes), it is also possible that smaller solutes may first form clusters with the solvent atoms. For example, solutes that bond more strongly to the solvent may be a more appropriate designation of the $\alpha$ solute. Since interatomic bond enthalpies are generally not known for condensed solids, this possibility has not yet been evaluated in detail. The relative interaction energies between Ca, Mg, and Zn atoms have been proposed based on estimated heats of mixing,[48] and show that the Ca-Zn interaction (−22 kJ/mol) is much stronger than the Ca-Mg and Mg-Zn interactions (−6 kJ/mol and −4 kJ/mol, respectively). Heats of mixing give a global representation of interatomic bond enthalpies that includes both the number of bonds formed and the energies of bonds between two atoms. Both the numbers of bonds and the energies of bonds are likely to be composition dependent so that the relative bond enthalpies obtained from heats of mixing should be used with caution. Nevertheless, the difference between the Ca-Zn interaction and the Ca-Mg and Mg-Zn interactions is sufficiently large to suggest that it may be appropriate to consider Zn as the $\alpha$ solute. The stronger preference for Zn atoms to avoid contact with other Zn atoms supports this assignment.

In the present work, Mg and Zn are each considered separately as $\alpha$ solutes. In the former case, a total solute atom fraction of 0.261 is required to fill the $\alpha$, $\beta$, and $\gamma$ sites, and in the latter case, a total solute fraction of 0.282 is needed. The ECP model predicts that no solute-solute nearest-neighbor pairs will be present in the amorphous structure with solute concentrations below these levels, and that the number of solute-solute neighbor pairs will increase with increasing solute concentration beyond these critical values. Considering either Zn or Mg as the $\alpha$ solute, the total solute content in the investigated alloys is sufficient to fill all the solute sites, with the remaining fraction occupying solvent sites. All four alloys show solute-solute bonding that vary in proportion to the solute concentration (Fig. 11), and this gives general agreement with the ECP model. More convincing support requires quantitative comparison of predicted PCNs from the ECP model with the values determined here. This requires specific assignment of the Mg and Zn solute atoms to $\alpha$, $\beta$, and $\gamma$ solute sites and to solvent sites. Topological models required for this comparison are not yet available but the data in the present work are expected to give important insights into development of such models.

## V. CONCLUSIONS

(1) A combination of neutron and x-ray diffraction and Reverse Monte Carlo modeling allowed the amorphous structure of $Ca_{60}Mg_XZn_{40-X}$ alloys ($X=10$, 15, 20 and 25 at. %) to be studied. Six partial radial distribution functions were extracted which give a good description of both the experimental neutron and x-ray structure factors and total correlation functions of these alloys.

(2) Consistent with expectations from the efficient cluster packing model, the amorphous structure of Ca-Mg-Zn MGs is shown to be describable as a mixture of Mg- and Zn-centered clusters, with Ca dominating in the first coordination shell of these clusters. A CN of 10 [$\sim$7 Ca+3(Mg+Zn)] is the most common for Zn-centered clusters whereas CN=11 and 12 [$\sim$7–8 Ca+4(Mg+Zn)] are the most common for Mg-centered clusters. Ca-centered clusters typically have CN=13.

(3) Analysis of the Voronoi polyhedra in the structural models demonstrates that there is a link between the clusters present in crystalline $CaMg_2$, and the glasses. As the concentration of Mg in the glass is increased there is a corresponding increase in the fraction of polyhedra which are both 12 coordinated and have a predominance of fivefold bond vertices. This change drives the structure toward the (0,0,12,0) polyhedra found in the crystal structure and explains the reduction in the GFA. Similar changes are noticed in the Ca environment but no specific links can be made between the changes in the Zn environment with composition and the preferential formation of CaZn.

(4) Efficient atomic packing is shown around the solute Mg and Zn atoms, where the Ca, Mg, and Zn atoms in the first coordination shells occupy all of the space available. Packing around Ca atoms is less efficient. The degree of packing efficiency around the solvent atom is suggested to contribute to glass-forming ability.

(5) Bond-angle distributions suggest near-equilateral triangles and pentagonal bipyramids to be the most common atom configurations. While fivefold bond configurations (pentagonal pyramids) are still populous ($\sim$60%) in the first coordination shell of the clusters, the characteristic solute (Mg or Zn) centered clusters are not icosahedral.

(6) Similar to oxide glasses and a binary Pd-Si BMG, Ca-Mg-Zn glasses contain short-range topological structures similar to those in their competing crystalline compounds. Some nearest-neighbor bond lengths are shorter in these glasses than in the competing crystals, suggesting that optimal short-range atomic packing is retained in metallic glasses since the long-range order constraint imposed by a crystalline structure is not present.

(7) An *ab initio* MD simulation, although for a small number of atoms, corroborates the structural findings above. The extensive structural characterization reported in this work thus offers a comprehensive account of the structure in Ca-Mg-Zn glasses, representing a category of MGs (alkaline-earth-metal based) that has not been well studied before.

## ACKNOWLEDGMENTS

Technical support from J. Michael Scott and Michael Braginsky and extensive discussions with Alexander Kolesnikov and Wojtek Dmowski are recognized. Neutron and x-ray experiments at the ISIS Pulsed Neutron and Muon Source were supported by a beamtime allocation (RB 820097) from the Science and Technology Facilities Council. Work at the Air Force Research Laboratory was supported through the Air Force Office of Scientific Research (Joan Fuller, Program Manager) and the Air Force under on-site Contract No. FA8650-10-D-5226 conducted through UES, Inc. Dayton, Ohio. Work at John Hopkins University was supported through the National Science Foundation under Contract No. NSF-DMR 0904188.

---

*Corresponding author. Phone: 1-937-255-1320; FAX: 1-937-656-7292; oleg.senkov@wpafb.af.mil

[1] O. N. Senkov and J. M. Scott, Scr. Mater. **50**, 449 (2004).

[2] O. N. Senkov and J. M. Scott, J. Non-Cryst. Solids **351**, 3087 (2005).

[3] O. N. Senkov, J. M. Scott, and D. B. Miracle, J. Alloys Compd. **424**, 394 (2006).

[4] O. N. Senkov, J. M. Scott, and D. B. Miracle, Intermetallics **14**, 1055 (2006).

[5] O. N. Senkov, J. M. Scott, and D. B. Miracle, Mater. Trans. **48**, 1610 (2007).

[6] O. N. Senkov, D. B. Miracle, V. Keppens, and P. K. Liaw, Metall. Mater. Trans. A **39**, 1888 (2008).

[7] V. Keppens, Z. Zhang, O. N. Senkov, and D. B. Miracle, Philos. Mag. **87**, 503 (2007).

[8] O. N. Senkov and D. B. Miracle, Metall. Mater. Trans. A **41**, 1677 (2010).

[9] *Handbook of Ternary Alloy Phase Diagrams*, edited by P. Villars, A. Prince, and H. Okamoto (ASM International, Materials Park, OH, 1995), p. 7522.

[10] S. Gorsse, G. Orveillon, O. N. Senkov, and D. B. Miracle, Phys. Rev. B **73**, 224202 (2006).

[11] X. D. Wang, S. Yin, Q. P. Cao, J. Z. Jiang, H. Franz, and Z. H. Jin, Appl. Phys. Lett. **92**, 011902 (2008).

[12] Y. Q. Cheng, H. W. Sheng, and E. Ma, Phys. Rev. B **78**, 014207 (2008).

[13] Y. Q. Cheng, E. Ma, and H. W. Sheng, Phys. Rev. Lett. **102**, 245501 (2009).

[14] V. Yu. Kazimirov, D. Louca, M. Widom, X. J. Gu, S. J. Poon, and G. J. Shiflet, Phys. Rev. B **78**, 054112 (2008).

[15] H. W. Sheng, W. K. Luo, F. M. Alamgir, J. M. Bai, and E. Ma, Nature (London) **439**, 419 (2006).

[16] H. W. Sheng, Y. Q. Cheng, P. L. Lee, S. D. Shastri, and E. Ma, Acta Mater. **56**, 6264 (2008).

[17] N. P. Bailey, J. Schiotz, and K. W. Jacobsen, Phys. Rev. B **69**, 144205 (2004).

[18] P. Jóvári, K. Saksl, N. Pryds, B. Lebech, N. P. Bailey, A. Mellergård, R. G. Delaplane, and H. Franz, Phys. Rev. B **76**,

054208 (2007).

[19] O. N. Senkov and D. B. Miracle, Mater. Res. Bull. **36**, 2183 (2001)

[20] D. B. Miracle, Nature Mater. **3**, 697 (2004); Acta Mater. **54**, 4317 (2006).

[21] O. N. Senkov and D. B. Miracle, in *Processing and Fabrication of Advanced Materials XIV*, edited by T. S. Srivatsan, R. A. Varin, R. Abbaschian, and S. Viswanathan (Materials Science and Technology, Pittsburgh, PA, 2005), pp. 249–266.

[22] D. B. Miracle, D. Louzguine-Luzgin, L. Louzguina-Luzgina, and A. Inoue, Int. Mater. Rev. **55**, 218 (2010).

[23] A. C. Hannon, Nucl. Instrum. Methods Phys. Res. A **551**, 88 (2005).

[24] A. K. Soper (private communication); GUDRUN software, http://www.isis.stfc.ac.uk/instruments/sandals/data-analysis/gudrun8864.html

[25] GUDRUNX software, http://www.isis.stfc.ac.uk/support-laboratories/xrd/data-analysis/xrd-data-analysis9203.html

[26] A. C. Hannon, W. S. Howells, and A. K. Soper, Inst. Phys. Conf. Ser. **107**, 193 (1990).

[27] D. A. Keen, J. Appl. Crystallogr. **34**, 172 (2001).

[28] E. Lorch, J. Phys. C **2**, 229 (1969).

[29] R. L. McGreevy, J. Phys.: Condens. Matter **13**, R877 (2001).

[30] M. G. Tucker, D. A. Keen, and A. C. Hannon (private communication).

[31] D. A. Keen and R. L. McGreevy, Nature (London) **344**, 423 (1990).

[32] O. Senkov, D. Miracle, and E. Barney, Invited talk at the Symposium on Bulk Metallic Glasses VII. TMS 2010 Annual Meeting & Exhibition, Seattle, WA, 14–18 February, 2010 (unpublished).

[33] http://www.rmc-forum.org/downloads/useful

[34] N. N. Greenwood and A. Earnshaw, *Chemistry of the Elements*, 2nd ed. (Butterworth-Heinemann, Oxford, UK, 1997).

[35] B. Cordero, V. Gómez, A. E. Platero-Prats, M. Revés, J. Echeverría, E. Cremades, F. Barragán, and S. Alvarez, Dalton Trans., **2008**, 2832.

[36] J. L. C. Daams, P. Villars, and J. H. N. van Vucht, *Atlas of Crystal Structure Types for Intermetallic Phases* (ASM International, Materials Park, OH, 1991), Vols. 1-4.

[37] R. Zallen, *The Physics of Amorphous Solids* (Wiley-VCH, Weinheim, 2004).

[38] D. B. Miracle, J. Non-Cryst. Solids **342**, 89 (2004).

[39] D. B. Miracle, W. S. Sanders, and O. N. Senkov, Philos. Mag. **83**, 2409 (2003).

[40] D. B. Miracle, E. A. Lord, and S. Ranganathan, Mater. Trans., JIM **47**, 1737 (2006).

[41] J. D. Bernal, Proc. R. Soc. London, Ser. A **280**, 299 (1964).

[42] D. R. Nelson, Phys. Rev. B **28**, 5515 (1983).

[43] F. C. Frank and J. S. Kasper, Acta Crystallogr. **11**, 184 (1958).

[44] J. L. Finney, Proc. R. Soc. London, Ser. A **319**, 495 (1970).

[45] P. H. Gaskell, Nature (London) **276**, 484 (1978).

[46] A. S. Clarke and H. Jonsson, Phys. Rev. E **47**, 3975 (1993).

[47] G. Kresse and J. Furthmuller, Phys. Rev. B **54**, 11169 (1996).

[48] A. Takeuchi and A. Inoue, Mater. Trans., JIM **46**, 2817 (2005).